# THE RADIATIVE IMPACT OF WATER ICE CLOUDS FROM ASSIMILATION OF MARS CLIMATE SOUNDER DATA

**L. J. Steele, S. R. Lewis, M. R. Patel**, *Department of Physical Sciences, The Open University, Walton Hall, Milton Keynes, MK7 6AA, UK (liam.steele@open.ac.uk),* **L. Montabone**, *Space Science Institute, Boulder, CO, USA/Department of Physics, University of Oxford, UK/Laboratoire de Météorologie Dynamique, IPSL, Paris, France,* **F. Forget**, *Laboratoire de Météorologie Dynamique, IPSL, Paris, France*.

**Introduction:**

Here we investigate the radiative impact of martian water ice clouds on the atmospheric temperature and circulation via the assimilation of Mars Climate Sounder (MCS) temperature and ice opacity profiles, and dust optical depths, into a Global Climate Model (GCM).

Recent observational and modelling studies have begun to reveal the importance of water ice clouds in terms of modifying the atmospheric temperature structure. Studies of temperature inversions observed by Mars Pathfinder and Mars Global Surveyor [Magalhães *et al*., 1999; Hinson and Wilson, 2004], surface temperature anomalies in Thermal Emission Spectrometer (TES) retrievals [Wilson et al., 2007], and more recently MCS observations [Kleinböhl *et al*., 2013] all suggest that clouds have important roles to play, providing local heating and cooling depending on location and time of day. Additionally, assimilation of Thermal Emission Spectrometer temperature profiles by Wilson *et al*., [2008] revealed the importance of clouds in modifying the temperature structure in the tropics.

Modelling studies using both 1D microphysical models and Global Climate Models (GCMs) have shown that cloud radiative effects can account for the observed temperature inversions [Colaprete and Toon, 2000], and have also demonstrated the role they play in intensifying thermal tides [Hinson and Wilson, 2004; Kleinböhl *et al*., 2013]. Cloud radiative effects have also been shown to increase temperatures in the tropics, and modify the meridional circulation, producing additional indirect changes to the atmospheric temperature structure [Madeleine *et al*., 2012]. However, as the radiative impact of clouds is dependent upon the location and time of day in which they form, the results of modelling studies will be affected by any incorrect predictions of cloud locations and opacities.

The assimilation procedure allows the ice opacity observations to be inserted into the model at their correct time and location, and with the correct opacity, producing the best state from which to analyze cloud radiative forcing. The resulting assimilated data set (covering all latitudes, longitudes and times) allows a detailed study of the atmospheric state that is not possible by using observations or models alone. The increased vertical coverage of the MCS temperature retrievals (~85 km) compared to the TES retrievals (~40 km) also allows the radiative effects of clouds to be studied to much higher altitudes than has previously been possible.

**MCS data and assimilation method:**

*Mars Climate Sounder data.* The data assimilated are temperature and ice opacity profiles from the MCS instrument aboard the Mars Reconnaissance Orbiter (MRO) spacecraft. The profiles are obtained from the surface to ~85 km (~0.1 Pa), with a vertical resolution of ~5 km [McCleese *et al*., 2010]. The observations comprise two sets of twelve narrow strips of data per sol, separated by ~30° in longitude, and due to the sun-synchronous orbit of MRO they occur at local times around 3 am and 3 pm The period chosen for this study is Mars year 30 as there are less gaps in the data, and there are between 1000–2500 vertical profiles available for assimilation each sol (see Figure 1).

Prior to assimilation the ice opacities per km obtained from the MCS data are converted from infrared (12 μm) to visible (670 nm) using the multiplicative factor 3.1, and are then interpolated to layer opacities on a set of 21 pressure levels spaced 5 km apart and ranging from −10 km to 95 km (with the 610 Pa corresponding to $z$ = 0 km).

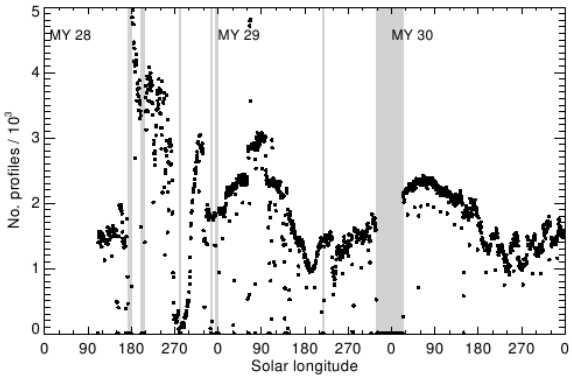


**Figure 1.** The number of ice opacity profiles retrieved each sol between $L_S$ = 110°, MY28 and $L_S$ = 360°, MY30. The grey shading represents periods greater than five sols where there is no data.

*Global Climate Model.* The GCM used for this study results from a collaboration between the Laboratoire de Météorologie Dynamique (LMD), the University of Oxford and The Open University. The model combines the most recent LMD physical schemes (including a two-moment dust transport scheme and thermal plume model; see Madeleine *et al*. [2011]; Colaitis *et al*. [2013]) with a spectral dynamical core, energy and angular-momentum conserving vertical finite-difference scheme and semi-Lagrangian advection scheme [see Lewis *et al*., 2007]. The model is run with a physical grid resolu-

tion of 5° in latitude and longitude, and there are 35 vertical levels in sigma coordinates ($\sigma = p/p_{surf}$) extending to ~100 km. For the current study there is no water cycle included in the simulations, as we wish to analyze the radiative impact of clouds compared to a cloud-free atmosphere.

*Data assimilation method.* The data assimilation scheme is a modified form of the Analysis Correction (AC) scheme, originally developed for use at the UK Met Office [Lorenc *et al*., 1991] and later re-tuned for martian conditions [Lewis *et al*., 1997], and verified using independent radio occultation data [Montabone *et al*., 2006]. Temperature profiles are assimilated with the method used previously for TES assimilations, with temperatures compared in the form of layer thicknesses [Lewis *et al*., 2007].

For the ice opacity assimilation, the layer opacities in each profile are interpolated from observation levels to model levels (assuming the opacity varies linearly with $\ln p$), and then the opacity increment at each level is calculated. Vertical interpolation is then performed to fill any levels where there is missing data between observations, and extrapolation is used to fill any levels with missing data above or below the highest and lowest observation levels with valid data. The extrapolation procedure uses the tail of a Gaussian, which allows the spreading of data to one or more model levels, but accounts for the fact that ice clouds can form in shallow discrete layers.

In order to use the assimilated ice opacities to calculate heating rates, the effective radius $r_{eff}$ and variance $\nu_{eff}$ of the ice particles need to be supplied for each grid box. The MCS opacity retrievals provide no data on particle sizes, as the radiative transfer scheme assumes a modified gamma distribution with the parameters $r_{eff}$ = 1.4 μm and $\nu_{eff}$ = 0.15 at all locations and seasons [Kleinböhl *et al*., 2011]. These values were chosen as a compromise between the wide range of observed particle sizes, and are the values we will use for this study. Figure 2 shows the zonally-averaged water ice optical depth resulting from the MY30 assimilation.

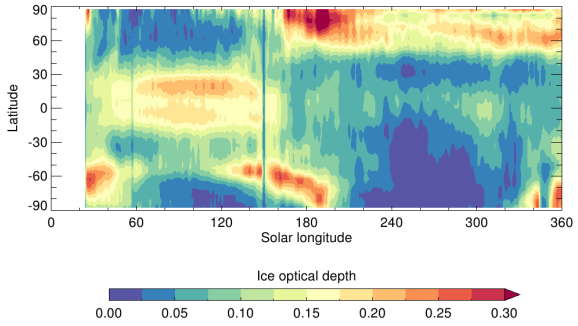


**Figure 2.** Zonally averaged visible water ice optical depth from an assimilation of MCS opacity profiles during MY 30. No data is available at the start of the year, or for two short periods at $L_S$ = 57° and between $L_S$ = 149°–150°.

**The radiative impact of clouds:** In order to assess the radiative impact of clouds on the atmospheric temperature structure and circulation, the results of an assimilation of ice opacities are compared to those from a control run, in which dust and $CO_2$ are the only atmospheric constituents influencing the radiative transfer, with the dust mass and number mixing ratios transported using a two-moment scheme [Madeleine *et al*., 2011]. Comparisons are made during northern summer ($L_S$ = 90°–120°), autumn ($L_S$ = 180°–210°) and winter ($L_S$ = 270°–300°).

The impact of the assimilated clouds on atmospheric temperatures can be seen in Figure 3. During northern summer (panels a,d,g) the aphelion cloud belt (ACB) is at its maximum opacity, the south polar hood (SPH) is at a low opacity in between its two distinct phases [Benson *et al*., 2010] and the north polar hood (NPH) is only beginning to form. During northern autumn (panels b,e,h) the NPH and SPH are at their maximum optical depths while the tropical clouds have reduced in opacity and increased in height. During northern winter (panels c,f,i) the NPH is still prominent while the SPH has disappeared, and some clouds remain over the tropics. The temperature changes seen are the result of both the direct radiative impact of clouds, as well as the indirect impact due to changes in the atmospheric circulation.

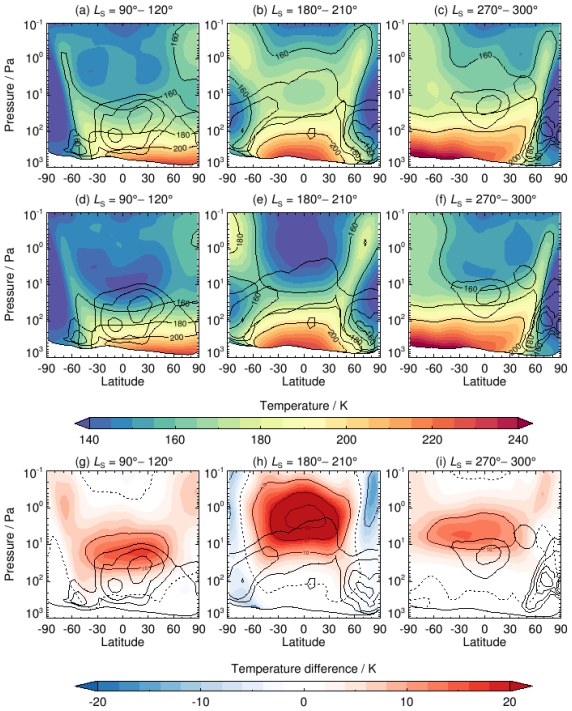


**Figure 3.** Zonal mean temperatures from the ice assimilation (IA, upper panels), control run (CR, middle panels), and the temperature difference $T_{IA}-T_{CR}$ (lower panels). Thick black contours show the assimilated visible ice opacity, with values of 0.005, 0.01, 0.02 and 0.03. Dotted contours in the lower panels denote zero temperature difference.

*Direct radiative impact.* It can be seen from the temperature differences (Figure 3, panels g–i) that the presence of clouds over the tropics leads to an increase in temperatures both at and above cloud-forming height. The temperature increase is around 10–15 K during northern summer and winter, and >30 K during northern autumn, even though the tropical cloud optical depth at this time is only around half that of the ACB peak. This increased heating during northern autumn is the result of the clouds in the tropics extending to higher altitudes, resulting in much larger density-scaled opacities, and it is these which are important in terms of heating [see e.g. Heavens *et al*., 2010].

The polar hood clouds are generally the most optically thick clouds (see Figure 2), but they appear to have very little impact on the local atmospheric temperature structure. During northern autumn and winter the addition of clouds results in temperatures over the north pole around 2–4 K cooler than an atmosphere with no clouds. Over the south pole during northern autumn the temperature difference is a little greater, with a cooling of around 6–8 K at and below the SPH. There are two main reasons for the small radiative impact of the polar hoods. Firstly, while the opacities are large, the clouds form at low altitudes in a denser atmosphere, and thus have smaller density-scaled opacities compared to the tropical clouds. Secondly, the surface temperatures and temperature difference between the surface and cloud-forming height are much less over the poles during autumn and winter than over the equator, and so the absorption of upwelling radiation by clouds over the poles produces substantially lower heating rates.

These lower heating rates can be seen in Figure 4, which show the longwave and shortwave heating rate differences between the IA and CR for both nighttime (3 am) and daytime (3 pm). As can be seen, the tropical clouds produce daytime longwave heating rates between around 10–25 K sol$^{-1}$ during both northern summer and winter, and >30 K sol$^{-1}$ during northern autumn. At night they emit radiation, leading to local cooling rates of around 5–10 K sol$^{-1}$. Both polar hoods produce minimal longwave cooling rates of around 0–2 K sol$^{-1}$.

In the shortwave range, the IA tropical daytime heating rates are higher than the CR by up to 5 K sol$^{-1}$ during northern summer and winter, and up to 10 K sol$^{-1}$ during autumn. However, some of this additional heating is caused by increased quantities of dust due to circulation changes, as opposed to being directly cloud-related. As the polar hood clouds form in the autumn and winter, there is little-to-no solar radiation available to be intercepted by the clouds. As such, shortwave heating rates are only a few K sol$^{-1}$ at the equatorward edges of the polar hoods during autumn.

*Indirect radiative impact.* The inclusion of cloud radiative effects generally results in a strengthening of the overturning cells in each period, with around a 50% increase in transport away from the centres of the cells, and peak increases approaching 200% in the upwelling and downwelling branches.

As well as re-distributing atmospheric constituents, the increasing strength of the meridional circulation also affects the strength of the polar warmings, with peak temperatures increased by around 6–8 K. The temperature changes associated with clouds result in changes to the meridional temperature gradients, leading to changes in the strength of jets. In the autumn and winter hemispheres, the cores of the westerly jets are strengthened by around 10–20 m s$^{-1}$, while over the equator during autumn the easterly jet speed is reduced, with the core speed decreasing from >100 m s$^{-1}$ to ~40 m s$^{-1}$.

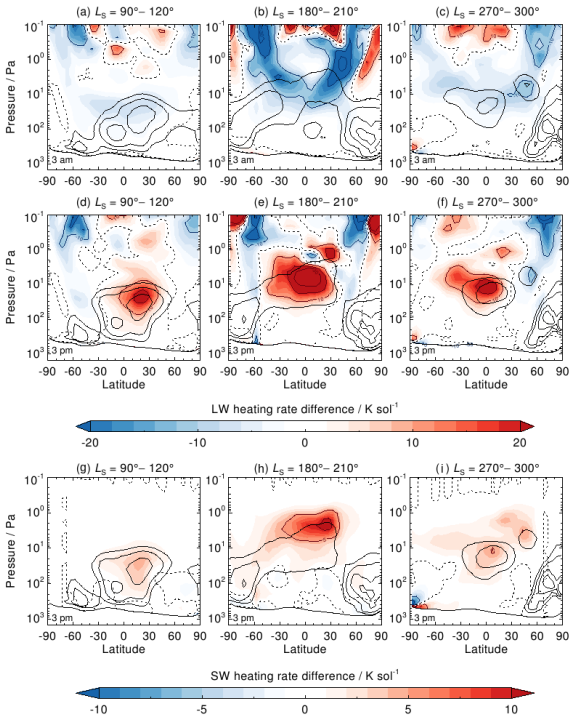


**Figure 4.** Zonal mean heating rate difference between an ice assimilation and control run ($H_{IA}$ - $H_{CR}$) for both longwave (5-200 μm, panels a-f, 3 am and 3 pm local times) and shortwave (0.1-5 μm, panels g-i, 3 pm local time only) radiation. Dotted contours denote zero heating rate difference, while thick black contours show the assimilated visible ice opacity.

**Summary:** Assimilations of MCS temperature and ice opacity profiles have been studied to investigate the radiative impact of water ice clouds. Tropical clouds are shown to produce local daytime heating rates between 10–20 K sol$^{-1}$, and nighttime cooling rates around 5 K sol$^{-1}$. The net result is an increase in atmospheric temperatures by 10–15 K around the 10 Pa pressure level. Polar hood clouds only have a small radiative impact compared to tropical clouds. A value of $r_{eff}$ = 1.4 μm provides good results for the ACB radiative effects, but for high-altitude tropical clouds during northern autumn

a better agreement with MCS observations is found using $r_{eff}$ = 0.8 μm, suggesting these clouds are composed of smaller particles than the ACB.

Clouds also have an indirect radiative effect, with the strengthening of the overturning cells producing increased polar warmings by around 6–8 K. Jet speeds are also modified through changes to the meridional temperature gradient, with the cores of the winter hemisphere westerly jets increasing by around 10–20 m $s^{-1}$, and the equatorial easterly jet weakening by around 60 m $s^{-1}$. The changing circulation also leads to redistribution of atmospheric constituents, further impacting temperature changes. The reduction of the effective radius to 0.8 μm during northern autumn also improves the magnitude and position of the polar warming due to the altered meridional circulation.

**Future work:** While the radiative impact of clouds has led to many improvements in the modelled atmospheric temperature structure, there are still biases present when compared to an assimilation of MCS temperature profiles. Many of these biases can be improved by using different ice particle effective radii in the radiative transfer calculations. Thus, the next stage is to couple the ice opacity assimilation to a model including an active water cycle. This will allow for variation of the effective radii with height, location and time, which should give further improvements to the modelled temperature structure, particularly the locations and strengths of the polar warmings. The water cycle coupling will also allow the interaction between the water and dust cycles to be studied in detail.

**Acknowledgements:** The authors acknowledge the support of the MCS science team. L. J. Steele is funded by the UK Science and Technology Facilities Council. L. Montabone is partly supported by the US National Aeronautics and Space Administration under Grant No. NNX13AK02G issued through the Mars Data Analysis Program 2012.

**References:**

Benson, J. L., D. M. Kass, A. Kleinböhl, D. J. McCleese, J. T. Schofield, and F. W. Taylor (2010), Mars' south polar hood as observed by the Mars Climate Sounder, J. Geophys. Res. (Planets), 115, E12015.

Colaitis, A., A. Spiga, F. Hourdin, C. Rio, F. Forget, and E. Millour (2013), A thermal plume model for the Martian convective boundary layer, J. Geophys. Res. (Planets), 118, 1468–1487.

Colaprete, A., and O. B. Toon (2000), The radiative effects of Martian water ice clouds on the local atmospheric temperature profile, Icarus, 145, 524–532.

Heavens, N. G., J. L. Benson, D. M. Kass, A. Kleinböhl, W. A. Abdou, D. J. McCleese, M. I. Richardson, J. T. Schofield, J. H. Shirley, and P. M. Wolkenberg (2010), Water ice clouds over the Martian tropics during northern summer, Geophys. Res. Lett., 37, L18202.

Hinson, D. P., and R. J. Wilson (2004), Temperature inversions, thermal tides, and water ice clouds in the Martian tropics, J. Geophys. Res., 109, E01002.

Kleinböhl, A. J. T. Schofield, W. A. Abdou, P. G. J. Irwin, and R. J. de Kok (2011), A single-scattering approximation for infrared radiative transfer in limb geometry in the Martian atmosphere, J. Quant. Spectrosc. Radiat. Transfer, 112, 1568–1580.

Kleinböhl, A., R. J. Wilson, D. Kass, J. T. Schofield, and D. J. McCleese (2013), The semidiurnal tide in the middle atmosphere of Mars, Geophys. Res. Lett., 40, 1952–1959.

Lewis, S. R., M. Collins, and P. L. Read (1997), Data assimilation with a martian atmospheric GCM: an example using thermal data, Adv. Space Res., 19, 1267–1270.

Lewis, S. R., P. L. Read, B. J. Conrath, J. C. Pearl, and M. D. Smith (2007), Assimilation of thermal emission spectrometer atmospheric data during the Mars Global Surveyor aerobraking period, Icarus, 192, 327–347.

Lorenc, A. C., R. S. Bell, and B. MacPherson (1991), The Meteorological Office analysis correction data assimilation scheme, Quart. J. R. Meteor. Soc., 117, 59–89.

Madeleine, J.B., F. Forget, E. Millour, L. Montabone, and M. J. Wolff (2011), Revisiting the radiative impact of dust on Mars using the LMD Global Climate Model, J. Geophys. Res., 116, E11010.

Madeleine, J.B., F. Forget, E. Millour, T. Navarro, and A. Spiga (2012), The influence of radiatively active water ice clouds on the Martian climate, Geophys. Res. Lett., 39, L23202.

Magalhães, J. A., J. T. Schofield, and A. Seiff (1999), Results of the Mars Pathfinder atmospheric structure investigation, J. Geophys. Res., 104, 8943–8955.

McCleese, D. J. N. G. Heavens, J. T. Schofield, W. A. Abdou, J. L. Bandfield, S. B. Calcutt, P. G. J. Irwin, D. M. Kass,A. Kleinböhl, S. R. Lewis, D. A. Paige, P. L. Read, M. I. Richardson, J. H. Shirley, F. W. Taylor, N. Teanby, and R. W. Zurek, (2010), Structure and dynamics of the Martian lower and middle atmosphere as observed by the Mars Climate Sounder: Seasonal variations in zonal mean temperature, dust, and water ice aerosols, J. Geophys. Res. (Planets), 115, E12016.

Montabone, L., S. R. Lewis, P. L. Read, and D. P. Hinson (2006), Validation of martian meteorological data assimilation for MGS/TES using radio occultation measurements, Icarus, 185, 113–132.

Wilson, R. J., G. A. Neumann, and M. D. Smith (2007), Diurnal variation and radiative influence of Martian water ice clouds, Geophys. Res. Lett., 34, L02710.

Wilson, R. J., Lewis, S. R., Montabone, L., & Smith, M. D. (2008). Influence of water ice clouds on Martian tropical atmospheric temperatures. Geophys. Res. Lett, 35, L07202.